ADVANCED FUNCTIONAL MATERIALS
www.afm-journal.de

Check for updates

Plant Pollen-Derived Radiative Cooling: Eco-Synthetic Designs with Integrated Air-Gaps

You Jin Kim, Jingyu Deng, Munho Kim, and Nam-Joon Cho**

To prevent global warming and an excessive energy footprint, sustainable and innovative solutions are essential. Radiative cooling presents a promising approach, traditionally relying on additives like TiO_2, SiO_2, and MgO to promote cooling but raising environmental concerns. Learning from nature, an alternative solution utilizing natural pollen grains, processed through a traditional soap-making technique to produce a natural cooling paper is proposed. Introducing air-gap structures to improve sunlight reflectivity and maintain infrared emittance, the approach demonstrates significant cooling effects—6.6 °C by day and 8.1 °C by night in South Korea—without reliance on external energy inputs. Eco-synthetic design with integrated air-gaps technology offers an efficient cooling strategy, but also advances environmental sustainability by eliminating the need for synthetic additives. Representing a leap toward eco-friendly cooling, the approach emphasizes the potential of natural materials in addressing climate change challenges, aligning with the pursuit of sustainable development without an excessive energy footprint.

1. Introduction

Today, there's a pressing need for eco-friendly, sustainably produced materials with multifunctional capabilities.[1] Global warming has led to rising temperatures, increased evaporation, and shifts in rainfall patterns, particularly impacting urban areas due to the Urban Heat Island (UHI) effect.[2] To combat global warming,[3] we've relied on energy-intensive cooling systems, contributing to higher energy costs and environmental pollution through CO_2 emissions.[4,5]

Y. J. Kim, M. Kim
School of Electrical and Electronic Engineering
Nanyang Technological University
Singapore 639798, Singapore
E-mail: munho.kim@ntu.edu.sg

J. Deng, N.-J. Cho
School of Materials Science and Engineering
Nanyang Technological University
Singapore 639798, Singapore
E-mail: njcho@ntu.edu.sg

N.-J. Cho
Centre for Cross Economy
Nanyang Technological University
Singapore 639553, Singapore

The ORCID identification number(s) for the author(s) of this article can be found under https://doi.org/10.1002/adfm.202511893

DOI: 10.1002/adfm.202511893

In response, researchers have explored radiative cooling as an innovative solution,[6] which involves emitting heat as infrared (IR) radiation into outer space, taking advantage of the Earth's atmosphere's high transmittance in the 8–13 µm wavelength range.[7] This range aligns with the peak thermal radiation emitted by a black body according to Planck's law at a typical ambient temperature (300 K).[8]

For the past decade, researchers have developed various strategies to increase the cooling efficiency of radiative coolers made of various materials, including synthetic polymers (PE,[9] PDMS,[7] PTFE,[10] PVDF,[11] PMMA,[12] PET,[6] and PEO[13]), dielectric materials (Si_3N_4[14], HfO_2 and SiO_2),[6] and metals (Cu).[15] While these materials have shown promise in cooling performance, they also come with their own set of challenges and limitations. For example, synthetic polymers demonstrate excellent cooling properties but are predominantly derived from non-renewable petroleum sources, which raises environmental concerns due to their limited biodegradability[16] and recyclability.[17] On the other hand, materials like dielectrics,[6,14] and metals[15] offer benefits such as outstanding durability, electrical insulation properties, and efficient heat conduction. However, their production requires substantial energy inputs, contributing to the overall environmental carbon footprint of radiative cooling technologies.[18]

In recent investigations, biomaterial-based radiative cooling has emerged as a promising approach to address the challenges discussed earlier.[19] Notably, Zhu et al. achieved significant results with silk as a radiative cooling material, achieving a daytime cooling effect of −3.5 °C below ambient air temperature and a nighttime cooling effect of −7 °C below ambient temperature by incorporating Al_2O_3 nanoparticles into chemically modified silk.[20] This modification enhanced reflectivity in the ultraviolet (UV) region, aligning the nanoparticle diameter with the wavelength of light to be reflected. Cellulose-based radiative coolers have also garnered attention in research efforts. Gamage et al. demonstrated a daytime cooling effect of −4.9 °C below the inner chamber temperature,[21] while Jaramillo-Fernandez et al. achieved a daytime cooling effect of −5.5 °C below ambient air temperature using pure cellulose with a porous structure.[22] To further enhance cooling efficiency, researchers have introduced nanoparticles such as SiO_2,[12] MgO,[23] and TiO_2[24] to optimize thermal emission and solar reflectance. However, the inclusion

 © 2025 Wiley-VCH GmbH

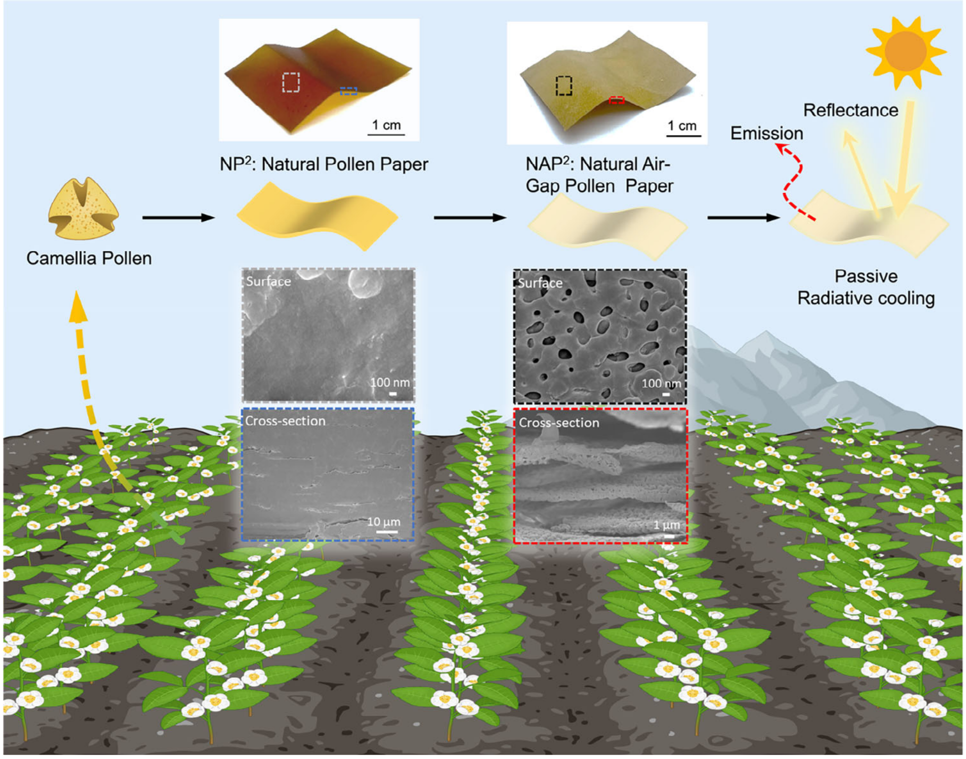

Figure 1. Schematic illustration of the pollen-based radiative cooler derived from nature. As a naturally abundant source, camellia pollen was used to fabricate natural pollen papers (NP^2) for radiative cooling. Based on this, the natural air-gap pollen paper (NAP^2) was formed via a freeze-drying process, which was a great candidate as a passive radiative cooler by introducing large amounts of nanopores on the surface and air-gaps in the cross-section.

of these nanoparticles raises concerns about potential environmental pollution, compromising the overall environmental sustainability of radiative cooling solutions.[25,26] Of particular note, TiO_2 nanoparticles have been associated with adverse effects, including lung inflammation and tumor formation.[27] This heightened toxicity and reactivity are attributed to the small sizes of nanoparticles, which exhibit an exponentially increased surface-to-volume ratio.[28]

Flowers in tropical environments have presented temperature adaptations in nature via transpiration and solar reflection to cool the environment.[29] Learning from nature, we were inspired by the biophysical characteristics of plant pollen as a choice of materials, which can help trap radiant heat and contribute to climate change.[30,31] Our strategy marks significant progress in radiative cooling technology, leveraging the natural properties of camellia pollen and eliminating the requirement for synthetic additives. Pollen grains are abundant in nature[32] and play a vital role in ecosystems,[33] known for their natural biodegradability.[34] Utilizing recent pioneering research to transform rigid raw pollen grains to soft microgels by the traditional soap-making process,[32] the microgel building blocks are the foundation for creating pollen papers through a simple evaporation technique.[35–37] To further enhance the properties of pollen paper, we have introduced air-gaps within the pollen paper layers using a freeze-dry casting method, effectively boosting reflectivity.[38] This innovation maximizes cooling efficiency under direct sunlight, spanning both the visible and near-infrared spectra, which collectively account for over 94% of the total solar spectrum energy according to AM 1.5 standards. The alternating refractive index between air gaps and pollen layers significantly enhance reflectivity, particularly benefiting daytime cooling applications.

We have demonstrated the impact of our approach across different climate conditions. In the mid-latitudes of South Korea, we have achieved a remarkable daytime cooling of ≈6.6 °C, with a further reduction in nighttime temperatures by 8.1 °C. In the tropical weather of Singapore, where intense sunlight and high humidity pose challenges that limit daytime cooling, our pollen-based radiative cooler still delivers a substantial 4.4 °C cooling effect during the night. Importantly, the unique air-gap structure with inherent chemical components of pollen allows it to serve as an efficient and sustainable radiative cooling solution, addressing eco-friendly footprint, sustainable production, and multifunctional capabilities for a sustainability goal.

2. Results and Discussion

2.1. Pollen Radiative Cooler Derived from Nature

Inspired by the natural radiative cooling strategy of flower plants and pollen,[29,31] pollen-derived materials were expected to contribute to the radiative cooling performance, involving their natural inherent properties, as presented in **Figure 1**. The natural air-gap pollen papers (NAP^2) were fabricated from the camellia sinensis pollen grains, renewable and naturally abundant materials.[35] The fabrication process is noninvasive and simple,

© 2025 Wiley-VCH GmbH

16163028, 0, Downloaded from https://advanced.onlinelibrary.wiley.com/doi/10.1002/adfm.202511893 by NANYANG TECHNOLOGICAL UNIVERSITY, Wiley Online Library on [21/07/2025]. See the Terms and Conditions (https://onlinelibrary.wiley.com/terms-and-conditions) on Wiley Online Library for rules of use; OA articles are governed by the applicable Creative Commons License

16163028, 0, Downloaded from https://advanced.onlinelibrary.wiley.com/doi/10.1002/adfm.202511893 by NANYANG TECHNOLOGICAL UNIVERSITY, Wiley Online Library on [21/07/2025]. See the Terms and Conditions (https://onlinelibrary.wiley.com/terms-and-conditions) on Wiley Online Library for rules of use; OA articles are governed by the applicable Creative Commons License

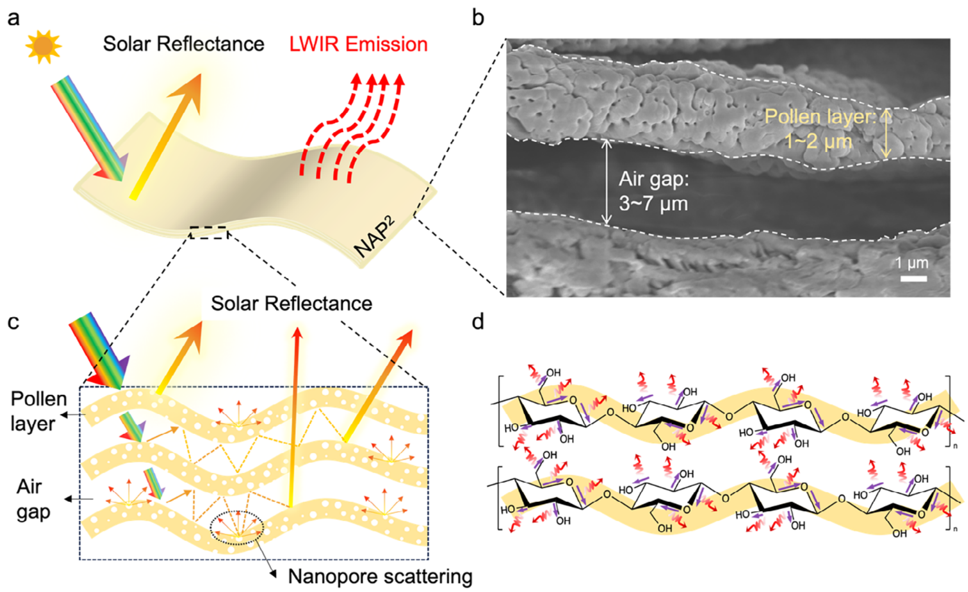

Figure 2. Mechanism analysis of natural air-gap pollen paper (NAP^2) as a radiative cooler. a) Illustration of solar reflectance and long-wave infrared (LWIR) emission on NAP^2. b) Cross-sectional FESEM images of NAP^2. c) Schematic of high reflectance in the vis–NIR range on NAP^2 through air-gap and nanopore scattering. d) Schematic of infrared emission by molecular vibration of the cellulose functional groups inside pollen particles.

transforming defatted camellia pollen grains into soft microgel particles through alkaline treatment as described previously.[32] This process induced de-esterification reactions in camellia sinensis pollen grains, leading to the emergence of numerous hydroxyl and carboxyl groups on the surface of the pollen microgel particles.[39] Following this, the existence of inherent nanopores on the hydrophilic pollen microgel particles' surface was unveiled through field emission scanning electron microscopy (FE-SEM) images (Figure S1a, Supporting Information). However, after forming natural pollen papers (NP^2) via ambient evaporation from pollen microgel suspension, the surface pores disappeared, leading to the tight assembly of pollen particles into densely structured layers.[35,36] Due to the abundance of hydrophilic functional groups on the surface of NP^2, the natural pollen papers readily absorbed water, trapping water molecules within the surface nanopores and the interstitial gaps between the layers of pollen particles.[37] After this water absorption, we further performed a freeze-drying process to maintain the nanopores and air-gaps to form natural air-gap pollen papers (NAP^2) (Figure S1b, Supporting Information). Camellia pollen paper presented great mechanical properties at ambient relative humidity (RH 60%), with the Young's modulus of NP^2 being around 0.54 GPa and that of NAP^2 being around 0.42 GPa, which ensured greater mechanical integrity during freeze-dry casting and stable outdoor cooling performance in Singapore (Figure S2, Supporting Information). Numerous studies have reported on radiative cooler research, focusing on multilayer thin films composed of metallic films (Au, Al) and dielectric materials (SiO_2, HfO_2) to achieve high reflection across the UV, visible, and IR spectra.[40] The construction of multilayered composites traditionally entails repeated cycles of material layering, leading to intricate manufacturing steps and elevated expenses.[41,42] In a departure from this conventional method,[42] our study harnessed naturally derived materials, specifically using the inherent properties of pollen paper to create a novel air-gap architecture via a simple freeze-drying and casting technique.[35] The NAP^2 presented a lighter appearance than NP^2, which was ascribed to the light scattering difference of the surface nanopores (Figure 1). The surface cross-sectional morphologies were detected and presented through FE-SEM, as shown in Figure 1. Large amounts of nanopores were observed on the surface of NAP^2, and air-gaps in sizes of 3–7 μm were found on the cross-sectional images of NAP^2, while the NP^2 displayed intact structures on both surface and cross-section.

2.2. Mechanism Analysis of Pollen Radiative Cooler

Incorporating the air-gap structure observed in the cross-section along with the chemical constituents derived from the intine layer of pollen in NAP^2, this mechanism has been thoroughly analyzed and explored as a promising approach for radiative cooling, as depicted in **Figure 2a**. Substantial air-gaps, ranging from 3 to 7 μm, were identified between layers of pollen particles in the cross-sectional views of NAP^2, as illustrated in Figure 2b. Concurrently, the inherent surface nanopores of camellia pollen particles, characterized by their distinct rough microarchitectures, were also revealed on the surface of each pollen layer in NAP^2, which contributed to the light scattering.

The unique structure of NAP^2 significantly enhanced the reflection of solar radiation by arranging alternating layers of air gaps and pollen material. The effectiveness of this arrangement can be attributed to the stark difference in refractive indices between pollen and air. Furthermore, the presence of intrinsic surface pores, with dimensions in the hundreds of nanometers, on NAP^2 facilitated an elevated reflection of visible light, spanning the 400–700 nm wavelength range. The synergy of abundant air-gaps and surface nanopores inherent to each pollen grain resulted in multiple internal reflections of light within NAP^2,

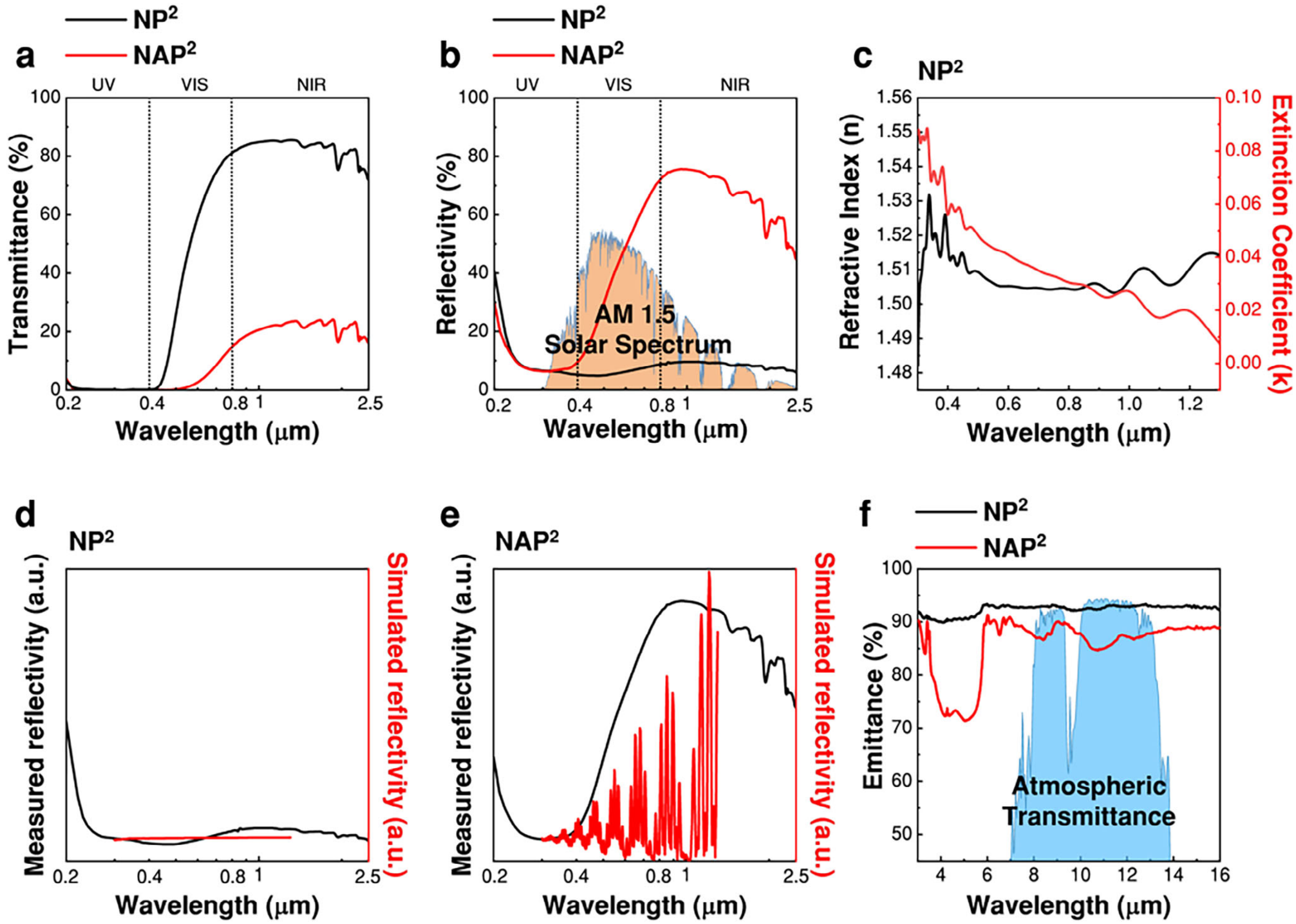

Figure 3. Optical properties of the pollen radiative cooler. a) Measured transmittance and b) reflectivity of NP^2 and NAP^2 using UV–vis spectroscopy along with AM 1.5 solar spectrum. c) Refractive index (n) and extinction coefficient (k) of NP^2. Comparison between measured and simulated reflectivity of d) NP^2 and e) NAP^2. f) Calculated emittance of NP^2 and NAP^2 along with atmospheric transmittance.

thereby significantly enhancing its radiative cooling capabilities, as detailed in Figure 2c. Additionally, cellulose-derived chemical structure, a primary constituent of the pollen's shell, along with sporopollenin, promotes robust infrared emissions through molecular vibrations and stretching, while also exhibiting strong UV light absorption, as depicted in Figure 2d. The distinctive air-gap configurations combined with the natural chemical makeup of pollen endow NAP^2 with exceptional qualities, positioning it as an advanced radiative cooling solution. This innovation offers considerable promise for sustainable development endeavors aimed at mitigating the global energy consumption crisis.

2.3. Optical Properties and Reflectivity Simulations

The strategic introduction of an air-gap structure into NP^2, transforming it into NAP^2, is a deliberate alteration designed to improve its radiative cooling efficiency when exposed to direct sunlight during the day. This modification leads to a significant decrease in the material's transmittance, indicating an enhanced capability to reflect sunlight and thereby reduce heat absorption (**Figure** 3a), accompanied by an increase in reflectivity (Figure 3b). This alteration can be ascribed to the variance in the refractive indices between pollen paper (≈1.5) and air (1), resulting in pronounced scattering effects in accordance with Snell's law.[43] The visibility and NIR transmission of NAP^2 markedly diminished across the 0.4–0.8 μm and 0.8–2.5 μm wavelength spans, respectively, as a consequence of enhanced reflectance within these specific wavelength intervals. Incorporating pores changed the semi-transparent NP^2 into opaque NAP^2, effectively blocking sunlight from heating the materials beneath the radiative cooler. Notably, the majority of solar energy is concentrated in the visible and NIR spectrums, as illustrated by the AM 1.5 solar spectrum.[44]

To explore how the air-gap structure contributes to increased reflectivity, we conducted finite-difference time-domain (FDTD) simulations, utilizing the empirically determined refractive index (n) and extinction coefficient (k) of NP^2 (Figure 3c). The schematic of the simulated structure for NAP^2 is provided in Figure S3 (Supporting Information), which is modeled after the cross-sectional FESEM image depicted in Figures 1 and 2. In our simulations, we specified the thickness of the pollen layer to be 1–2 μm and that of the air-gap to be 3–7 μm. Reflectivity simulations with variations in the thickness of pollen layers and air gaps are

© 2025 Wiley-VCH GmbH

16163028, 0, Downloaded from https://advanced.onlinelibrary.wiley.com/doi/10.1002/adfm.202511893 by NANYANG TECHNOLOGICAL UNIVERSITY, Wiley Online Library on [21/07/2025]. See the Terms and Conditions (https://onlinelibrary.wiley.com/terms-and-conditions) on Wiley Online Library for rules of use; OA articles are governed by the applicable Creative Commons License

also included in Figure S4 (Supporting Information). Parametric FDTD results predict maximum solar-band reflectance when the pollen layer is 1 μm thick and the inter-layer air-gap is 7 μm. Experimentally, only the sample freeze-dried at −196 °C develops such gaps (Figure S5, Supporting Information) and correspondingly shows the strongest reflectance enhancement (Figure S6, Supporting Information). It is worth noting that the freeze-dry casting technique employed not only succeeded in generating the targeted air-gap configuration but additionally induced the formation of pores within the pollen layers, averaging 300 nm in diameter (Figure S7, Supporting Information). In our simulation model for NAP^2, pores measuring 300 nm in diameter were incorporated. As shown in Figure 3d, the reflectivity of NP^2 simulated based on this model closely matched the observed reflectivity across the wavelength span of 0.3–1.3 μm, according to the measured values of refractive index (n) and extinction coefficient (k), highlighting the naturally low reflectivity of NP^2. Conversely, the simulated reflectivity for NAP^2 displayed a marked increase across the same wavelength range. The FDTD domain (0.3–1.3 μm) matches the wavelength range over which reliable n and k values were obtained by spectroscopic ellipsometry (J.A. Woollam M-2000); this window encompasses the vast majority of AM 1.5 solar energy. The simulation results comparing the reflectivity of the air-gap structure, both with and without pores, are detailed in Figure S8 (Supporting Information). The inclusion of pores in our simulation model led to a marginal increase in reflectivity. These simulation findings allow us to deduce that the improved reflectivity observed in NAP^2 can be mainly attributed to the air-gap structure, which emerges from the alternating refractive indices of pollen and air. Moreover, the incorporation of pores within the pollen not only augmented this effect but also amplified reflectivity via Mie scattering.[44] Figure 3f displays the emittance levels of NP^2 and NAP^2 in comparison with the atmospheric transmittance. Given that the Earth's atmosphere allows for high transmittance in the atmospheric window (8–13 μm), achieving effective radiative cooling necessitates that the cooler exhibits high emittance within this specific wavelength range. The high emittance was primarily attributed to the C─O stretching vibration in the acetyl group of pollen paper, which corresponds to the FTIR peak at 1216 cm^{-1}, positioned within the atmospheric window (Figure S9, Supporting Information).[45] Although NP^2 and NAP^2 share identical molecular composition, NP^2 shows a slightly higher emittance. This difference originates from geometry: the freeze-drying step introduces an air gap into NAP^2, lowering the areal density of IR-active C─O bonds and adding pollen/air interfaces that partially reflect LWIR photons. The trade-off is intentional, as introducing air-gaps sacrifices a few percent of LWIR emittance yet boosts solar-band reflectance, yielding an overall gain of enhanced cooling performance during daytime. This strategy enabled the achievement of effective daytime cooling by preserving the radiative cooling capacity while also enhancing reflectivity to minimize the absorption of incoming solar radiation.

2.4. Outdoor Cooling Performance

Figure 4a shows the outdoor measurement arrangement used to assess the radiative cooling effectiveness of NP^2 and NAP^2 in actual environmental conditions. NP^2 and NAP^2 were each placed in distinct acrylic chambers, both configured in the same manner. To avoid unintended increases in temperature inside the chambers, we wrapped them in aluminum foil. The radiative cooling devices were set on polystyrene foam to minimize convective heat transfer.[46] For insulation purposes, while still allowing for IR emission, the chambers were topped with NIR-transparent polyethylene (PE) film. Within the chamber, two thermocouples were installed: one situated between the cooling device and the polystyrene foam to monitor the temperature of the cooler, and the other located inside the chamber to measure the temperature within. A diagram illustrating the setup is provided in Figure S10 (Supporting Information). The outside ambient air temperature and relative humidity data were collected from the weather center with permission.[47,48] We measured the cooling performance of NP^2 and NAP^2 in two different locations in South Korea (Mid-latitudes 38.173° N, 128.584° E) and Singapore (Tropical 1.343° N, 103.681° E) (Figure 4b). In Figure 4c, we present the cooling performance measured in South Korea. The graph illustrates the temperature profiles of the Inner chamber, NP^2, NAP^2, and Ambient air, along with the temperature difference (dT) for NP^2 and NAP^2 compared to the Inner chamber temperature. The measurements were carried out over a span of 24 h, from 9:30 AM to the following day at 9:30 AM. At the onset of the measurement until around 10:50 AM, the temperature of the Inner chamber closely paralleled that of the ambient air. During this period, the dT values for NP^2 and NAP^2, compared to the Inner chamber temperature, were −5.2 and −5.7 °C, respectively. NAP^2 exhibited greater cooling during this time due to its heightened sunlight reflection capability in comparison to NP^2. After 11 AM, as direct sunlight began to heat up both the chamber and the coolers, the temperatures of NP^2, NAP^2, and the Inner chamber exhibited an upward trend. Around midday, NP^2's cooling effect disappeared as it absorbed sunlight, while NAP^2 sustained a cooling of −4 °C, showing its ability to remain cool under direct sunlight. NAP^2 reached its peak cooling performance of −6.6 °C around 2 PM, attributed to the combined effect of sunlight reflection from the air-gap structure and pores. After 3:30 PM, with the decline of direct sunlight, the temperatures of NP^2 and NAP^2 decreased. During the nighttime measurements, NP^2 and NAP^2 recorded dT values of −8.8 and −8.1 °C, respectively. NP^2's higher emittance in the atmospheric window contributed to a more pronounced cooling effect during the night because the absence of sunlight absorption and lower relative humidity further facilitated cooling (Figure S11, Supporting Information). Solar irradiance data for the Korean measurement are provided in Figure S12 (Supporting Information). When compared to the Ambient air temperature, NP^2 demonstrated a cooling effect of −10.4 °C, which persisted throughout the night until sunrise. This cooling effect extended to the Inner chamber, resulting in a temperature reduction of −4.3 °C compared to the Ambient air at 7:40 AM, as the cooler lowered the temperature of the Inner chamber. By presenting the cooling performance measured in South Korea, we demonstrate the cooler's ability to efficiently modulate temperature in a sustainable manner. Figure 4d presents the cooling performance measurements conducted in Singapore with the identical setup and methodology used for the measurement in South Korea. The data was collected from 5:40 PM to 08:30 AM, in a nighttime period on a clear sky with minimal cloud cover.

© 2025 Wiley-VCH GmbH

16163028, 0, Downloaded from https://advanced.onlinelibrary.wiley.com/doi/10.1002/adfm.202511893 by NANYANG TECHNOLOGICAL UNIVERSITY, Wiley Online Library on [21/07/2025]. See the Terms and Conditions (https://onlinelibrary.wiley.com/terms-and-conditions) on Wiley Online Library for rules of use; OA articles are governed by the applicable Creative Commons License

16163028, 0, Downloaded from https://advanced.onlinelibrary.wiley.com/doi/10.1002/adfm.202511893 by NANYANG TECHNOLOGICAL UNIVERSITY, Wiley Online Library on [21/07/2025]. See the Terms and Conditions (https://onlinelibrary.wiley.com/terms-and-conditions) on Wiley Online Library for rules of use; OA articles are governed by the applicable Creative Commons License

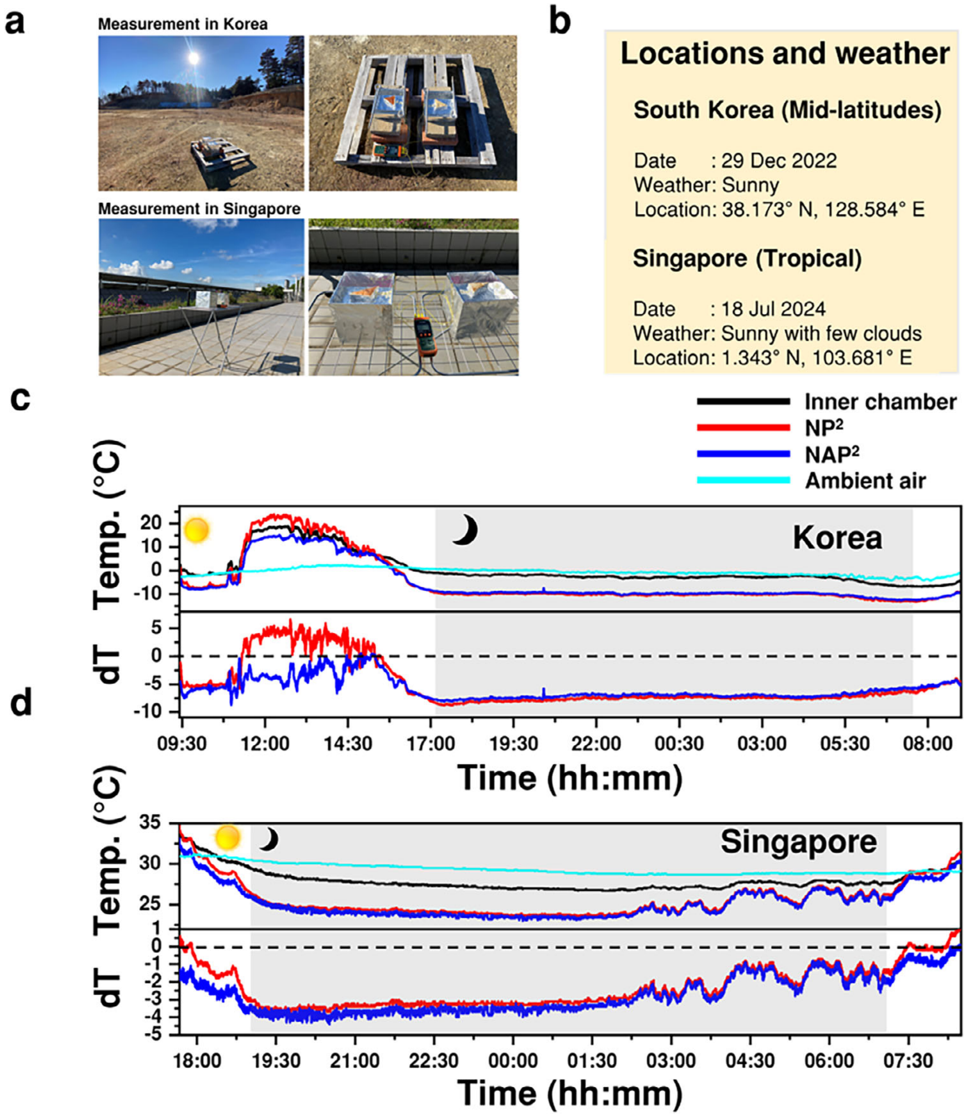

Figure 4. Measurement of the radiative cooling performance of NP^2 and NAP^2 in South Korea and Singapore. a) Photographs of the setup used for cooling performance measurements in Korea and Singapore. b) Details of the test locations, including geographical and meteorological information. Recorded temperatures of the inner chamber, NP^2, NAP^2, and the surrounding air, along with the temperature differential between the inner chamber and both NP^2 and NAP^2, in c) South Korea and d) Singapore.

A 24-h measurement of data can be found in Figure S13 (Supporting Information). The tropical weather in Singapore is challenging; the fluctuation observed in the daytime plot stems from variations in temperature caused by clouds, which block solar exposure.[49] In Singapore, while the assessments revealed that neither NP^2 nor NAP^2 displayed pronounced daytime cooling effects under direct sunlight, it's important to contextualize these findings within the region's unique environmental conditions. Singapore's tropical climate, characterized by intense solar irradiance and relatively high humidity levels—typically ranging from 70% to 80% during clear weather—presents a challenging scenario for passive cooling technologies. The high humidity contributes to additional atmospheric radiation, which can inhibit the effective passage of IR emissions through the atmospheric window. Despite these environmental challenges, the comparative analysis of the dT plots for NAP^2 and NP^2 offers a noteworthy insight: NAP^2 demonstrated a superior ability to reflect sunlight compared to NP^2. This observation underscores the potential of NAP^2 in enhancing passive cooling strategies, even in demanding climatic conditions. This marked distinction was evident in the daytime assessments conducted under direct sunlight, where the temperature of NAP^2 remained ≈6 °C lower than that of NP^2. Such findings highlight NAP^2's enhanced capability to reflect sunlight, contributing to its effectiveness in mitigating temperature increases during periods of intense solar exposure. This performance attribute of NAP^2 was further examined in the nighttime cooling evaluations carried out on July 18, 2024 (Figure 4d). NAP^2 demonstrated a reduction in temperature of 4.4 °C relative to the inner chamber and 6.4 °C in comparison to the ambient air temperature, despite the presence of 60–80% relative humidity

 © 2025 Wiley-VCH GmbH

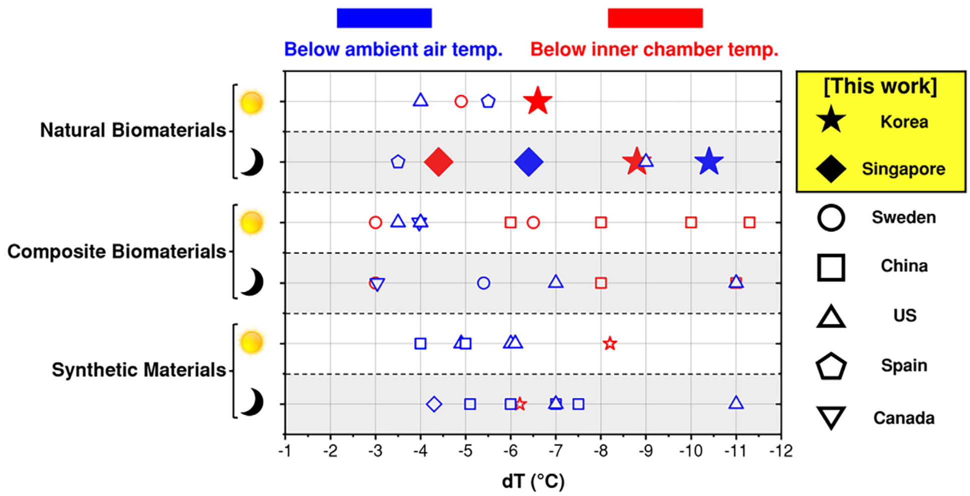

Figure 5. Benchmarking of cooling performance. Temperature difference of NAP^2 in comparison to the inner chamber and ambient air, along with a comparison to previously reported data. The data is categorized into three sections: Natural Biomaterials (i.e., cellulose, silk, wood, etc., without additives), Composite Biomaterials (i.e., biomaterials added with SiO_2, TiO_2, carbon black, etc., to enhance reflectivity), and Synthetic Materials (i.e., coolers made of synthetic polymers, metals, and semiconducting materials).

(Figure S14, Supporting Information). Additional cooling runs in Korea and Singapore, demonstrating the reproducibility of the cooling performance, are shown in Figure S15 (Supporting Information). This result underscores the efficacy of our pollen-based cooling technology in tropical climates after sunset, presenting a significant contribution to cooling strategies.

2.5. Comparative Assessment of Advanced Radiative Cooling Materials for Sustainable Cooling Efficiency

Figure 5 presents a comparative assessment of the cooling performance among various radiative cooler materials. In this graphical representation, the horizontal axis (x-axis) delineates the temperature differential, denoted as dT, while the vertical axis (y-axis) is utilized to classify radiative cooling materials into three main categories based on their compositional makeup: Natural Biomaterials, Composite Biomaterials, and Synthetic Materials. The variation in dT is visually distinguished using color coding: blue signifies a comparison to Ambient air temperatures, whereas red illustrates a comparison to temperatures within the Inner chamber. Furthermore, the specific sites of measurement are denoted by various symbols for clarity. Within the category labeled "Natural Biomaterials," the focus is on materials that are derived from natural sources—including pollen, cellulose, silk, and wood—without the incorporation of any synthetic additives, highlighting their pure and unaltered state. For the Composite Biomaterials category, the integration of biomaterials with additives such as SiO_2 and TiO_2 was employed to augment reflectivity and IR emission characteristics. The Synthetic Materials category encompasses radiative cooling devices fabricated from an array of synthesized entities, including synthetic polymers, metals, and semiconductors. The benchmarking figure with reference information is provided in Figure S16 (Supporting Information). Additionally, Figure S17 (Supporting Information) provides a comparison between the cooling performance of our work measured in Singapore and previously measured data from another group, also conducted in Singapore[49]. The establishment of a comparative assessment plot facilitates a straightforward juxtaposition of our cooling technology's performance against the forefront of achievements recently unveiled by various research collectives. Remarkably, the cooling efficacy of our specimen, as indicated by a pronounced value, stands out when compared to that of other Natural Biomaterials, hinting at its enhanced cooling prowess. Moreover, relative to the performance metrics of both Composite Biomaterials and Synthetic Materials, the majority of outcomes reveal diminished cooling capabilities when juxtaposed with our results. This underscores the import of our accomplishment, proposing a compelling cooling methodology rooted in natural biomaterials. Crucially, our strategy distinguishes itself as a viable, sustainable alternative, obviating the need for the incorporation of exogenous substances like SiO_2 or TiO_2 particles. This accentuates the capability of our radiative cooler to deliver effective temperature regulation while embracing sustainability and simplicity.

3. Conclusion

Our work pioneers a sustainable methodology for radiative cooling, leveraging natural materials. Through the innovative use of camellia pollen, we have showcased a radiative cooler that exhibits exceptional cooling capabilities with air-gap incorporation. This configuration, featuring alternating refractive indices between pollen and air, enhances sunlight reflectivity, thereby facilitating radiative cooling during daylight hours. Outdoor evaluation of NAP^2's cooling efficiency in South Korea, under direct sunlight conditions, revealed a peak cooling achievement of −6.6 °C relative to the internal chamber temperature. The air-gap structure significantly contributes to improved reflectivity across the visible and NIR spectrum, capturing the majority of solar energy influx. Remarkably, the integration of air-gap structures did not markedly impair the IR emittance of NAP^2 in the

© 2025 Wiley-VCH GmbH

16163028, 0, Downloaded from https://advanced.onlinelibrary.wiley.com/doi/10.1002/adfm.202511893 by NANYANG TECHNOLOGICAL UNIVERSITY, Wiley Online Library on [21/07/2025]. See the Terms and Conditions (https://onlinelibrary.wiley.com/terms-and-conditions) on Wiley Online Library for rules of use; OA articles are governed by the applicable Creative Commons License

atmospheric window, compared to NP^2, enabling NAP^2 to attain a notable cooling effect of −8.1 °C at night in Korea. Our approach foregrounds environmental sustainability by intentionally avoiding external additives, thus preserving the eco-friendly integrity of our innovation. By utilizing natural materials, we achieve notable cooling efficiency without compromising ecological overburden.

4. Experimental Section

Defatting of Camellia Bee Pollens: 500 g of camellia bee pollen (Shanxi GTL Biotech Co., Ltd) was mixed in deionized water (1 L, 50 °C) and stirred for 2 h. The pollen suspension was passed through a nylon mesh (pore size: 200 μm in diameter) to remove sand and contaminants. The remaining pollen grains were collected by vacuum filtration and mixed with acetone (1 L, room temperature). The mixture was stirred for 3 h (800 rpm) with an IKA disperser and vacuum filtered. The obtained pollen particles were washed 3–4 times with fresh acetone again until the filtrate became clear. The filtered pollen powders were left in the fume hood overnight (12 h) to evaporate the acetone fully. Thereafter, the dried pollen powder was dispersed and stirred in diethyl ether (1 L, room temperature) for 2 h. This process was repeated twice more. The pollen was then mixed with fresh diethyl ether (1 L, room temperature) and stirred overnight to complete the reactions. Finally, the pollen powder was transferred into a glass petri dish and left in the fume hood to fully dry and recover the defatted pollen powder.

Fabrication of NP^2 and NAP^2: Defatted pollen (20 g) was refluxed with aqueous 10 wt.% potassium hydroxide (KOH) (200 mL) solution (80 °C, 2 h) with stirring at 800 rpm. The suspension was collected using a nylon mesh for filtration (pore size: 30 μm) and then washed with fresh KOH solution (10 wt.%) until the filtrate was clear. Following this, the samples were incubated in fresh KOH solution (10 wt.%) at 80 °C for different incubation periods to undergo de-esterification, as previously reported[32]. Neutralization of the samples was then carried out with deionized (DI) water via the same nylon mesh (pore size: 35 μm) until the pH value reached around 7.5, forming pollen microgel. The resulting pollen microgel suspension was poured into a square Petri dish with lateral dimensions of 14 cm x 14 cm, followed by drying under an ambient environment for 5 days. Then, the NP^2 was obtained after peeling off from the petri dish. Afterward, the NP^2 was immersed in DI water for 15 mins to absorb water and swell completely, and the wet NP^2 was then frozen at −196 °C for 15 mins, followed by freeze-drying in a lyophilizer (Labcocon) for 48 h. Then, NAP^2 was formed after being removed from the lyophilizer.

Characterizations: The morphology and cross-sectional structures were characterized using a Field-Emission Scanning Electron Microscope (FESEM) (JSM-7600F Schottky field-emission scanning electron microscope). Samples were sputter-coated (JEOL) for 30 s under 40 kV before observation. Reflectance and transmittance spectra were tested by a UV–vis–NIR spectrometer (PerkinElmer Lambda 950) coupled with an internal integrating sphere (150 mm Spectralon). Fourier Transform infrared (FTIR) spectra of pollen samples were obtained with the PerkinElmer Spectrometer (PerkinElmer, UK) equipped with a diamond cell attenuated total reflection. Reflectance IR spectra were obtained between 4000 and 600 cm^{-1} by means of 16 scans per measurement. Background spectra were subtracted from each sample spectrum automatically by the Spectrum 10 Software (PerkinElmer, UK). To correct spectra with sloped baselines and reduce the amount of noise in the spectrum, a baseline correction and smoothing process was conducted after sample measurements using the software. Refractive index (n) and extinction coefficient (k) of NP^2 were obtained by ellipsometry measurement (M-2000 ellipsometer, J.A. Woollam). During measurement, the NP^2 was clamped at its coners with low-residue black Kapton tape to create a flat, specular area within the beam footprint (Figure S18, Supporting Information). The simulation of reflectivity for NP^2 and NAP^2 was carried out using Lumerical's finite-difference-time-domain (FDTD) method, based on the n, k values of NP^2. A plane-wave light source was utilized for normal incident illumination, and a perfectly matched layer (PML) was applied to the vertical ends, with the reflectance monitor positioned at the rear of the light source. The structure of NAP^2 was replicated based on the cross-sectional FE-SEM image of NAP^2. The infrared emittance spectra of NP^2 and NAP^2 were acquired by examining the infrared reflectance spectra using Fourier transform infrared spectroscopy (FTIR, PerkinElmer Spectrum 3TM) equipped with a gold integrating sphere (PerkinElmer Mid-IR Integrating sphere, featuring an 8° incident angle).

Cooling Performance Measurements: The measurements were conducted outdoors in both South Korea (38.173° N, 128.584° E) and Singapore (1.343° N, 103.681° E). NP^2 and NAP^2 were placed inside acrylic boxes, with aluminum foil attached to the box surface to reflect sunlight. A polyethylene film (16 μm) covered the top of the acrylic box for sealing. To minimize heat conduction, NP^2 and NAP^2 were positioned on polystyrene foam, and a 4-channel datalogging thermometer (SDL200, K-type, Extech) was employed to measure the temperatures of NP^2, NAP^2, and the inner chamber. Ambient air temperature, relative humidity, and wind speed data for the respective locations in Korea and Singapore were obtained from the Korea Meteorological Administration (Open Weather Data Portal) and the Meteorological Service Singapore, respectively, with permission.

Supporting Information

Supporting Information is available from the Wiley Online Library or from the author.

Acknowledgements

Y.J.K. and J.D. contributed equally to this work as the first authors. This work was supported by the Ministry of Education, MOE-MOET32022 (Grant no. 023126-00001), MOE AcRF Tier 1, RG111/20, and RG34/22.

Conflict of Interest

The authors declare no conflict of interest.

Data Availability Statement

The data that support the findings of this study are available from the corresponding author upon reasonable request.

Keywords

air-gap structure, bioinspired cooling technology, pollen-derived materials, radiative cooling, sustainable passive cooling

Received: May 12, 2025
Published online:

[1] C. Xu, T. A. Kohler, T. M. Lenton, J.-C. Svenning, M. Scheffer, *Proc. Natl. Acad. Sci.* **2020**, *117*, 11350.
[2] M. Burke, S. M. Hsiang, E. Miguel, *Nature* **2015**, *527*, 235.
[3] M. T. McCulloch, A. Winter, C. E. Sherman, J. A. Trotter, *Nat. Clim. Change* **2024**, *14*, 171.
[4] S. Chu, A. Majumdar, *Nature* **2012**, *488*, 294.
[5] X. Li, B. Sun, C. Sui, A. Nandi, H. Fang, Y. Peng, G. Tan, P.-C. Hsu, *Nat. Commun.* **2020**, *11*, 6101.
[6] A. P. Raman, M. A. Anoma, L. Zhu, E. Rephaeli, S. Fan, *Nature* **2014**, *515*, 540.

© 2025 Wiley-VCH GmbH

16163028, 0, Downloaded from https://advanced.onlinelibrary.wiley.com/doi/10.1002/adfm.202511893 by NANYANG TECHNOLOGICAL UNIVERSITY, Wiley Online Library on [21/07/2025]. See the Terms and Conditions (https://onlinelibrary.wiley.com/terms-and-conditions) on Wiley Online Library for rules of use; OA articles are governed by the applicable Creative Commons License

[7] L. Zhou, H. Song, J. Liang, M. Singer, M. Zhou, E. Stegenburgs, N. Zhang, C. Xu, T. Ng, Z. Yu, *Nat. Sustain.* **2019**, *2*, 718.
[8] X. Yin, R. Yang, G. Tan, S. Fan, *Science* **2020**, *370*, 786.
[9] Y. Peng, J. Chen, A. Y. Song, P. B. Catrysse, P.-C. Hsu, L. Cai, B. Liu, Y. Zhu, G. Zhou, D. S. Wu, *Nat. Sustain.* **2018**, *1*, 105.
[10] X. Wu, J. Li, F. Xie, X.-E. Wu, S. Zhao, Q. Jiang, S. Zhang, B. Wang, Y. Li, D. Gao, *Nat. Commun.* **2024**, *15*, 815.
[11] Y.-N. Song, M.-Q. Lei, J. Lei, Z.-M. Li, *Mater. Today Energy* **2020**, *18*, 100504.
[12] T. Suichi, A. Ishikawa, T. Tanaka, Y. Hayashi, K. Tsuruta, *Sci. Rep.* **2020**, *10*, 6486.
[13] D. Li, X. Liu, W. Li, Z. Lin, B. Zhu, Z. Li, J. Li, B. Li, S. Fan, J. Xie, *Nat. Nanotechnol.* **2021**, *16*, 153.
[14] Z. Chen, L. Zhu, A. Raman, S. Fan, *Nat. Commun.* **2016**, *7*, 13729.
[15] B. Bhatia, A. Leroy, Y. Shen, L. Zhao, M. Gianello, D. Li, T. Gu, J. Hu, M. Soljačić, E. N. Wang, *Nat. Commun.* **2018**, *9*, 5001.
[16] M. Ramesh, K. Palanikumar, K. H. Reddy, *Renew. Sustain. Energy Rev.* **2017**, *79*, 558.
[17] A. Samir, F. H. Ashour, A. A. Hakim, M. Bassyouni, *Npj Mater. Degrad.* **2022**, *6*, 68.
[18] Y. Jung, M. Kim, T. Kim, J. Ahn, J. Lee, S. H. Ko, *Nanomicro Lett.* **2023**, *15*, 160.
[19] H. Sun, F. Tang, Q. Chen, L. Xia, C. Guo, H. Liu, X. Zhao, D. Zhao, L. Huang, J. Li, *Chem. Eng. J.* **2023**, *455*, 139786.
[20] B. Zhu, W. Li, Q. Zhang, D. Li, X. Liu, Y. Wang, N. Xu, Z. Wu, J. Li, X. Li, *Nat. Nanotechnol.* **2021**, *16*, 1342.
[21] S. Gamage, D. Banerjee, M. M. Alam, T. Hallberg, C. Åkerlind, A. Sultana, R. Shanker, M. Berggren, X. Crispin, H. Kariis, *Cellulose* **2021**, *28*, 9383.
[22] J. Jaramillo-Fernandez, H. Yang, L. Schertel, G. L. Whitworth, P. D. Garcia, S. Vignolini, C. M. Sotomayor-Torres, *Adv. Sci.* **2022**, *9*, 2104758.
[23] P. Das, S. Rudra, K. C. Maurya, B. Saha, *Adv. Mater. Technol.* **2023**, *8*, 2301174.
[24] J. Mandal, Y. Yang, N. Yu, A. P. Raman, *Joule* **2020**, *4*, 1350.
[25] Z. Yang, Z. Liu, R. Allaker, P. Reip, J. Oxford, Z. Ahmad, G. Ren, *J. R. Soc. Interface* **2010**, *7*, S411.
[26] M. Sajid, M. Ilyas, C. Basheer, M. Tariq, M. Daud, N. Baig, F. Shehzad, *Environ. Sci. Pollut. Res.* **2015**, *22*, 4122.
[27] V. Freyre-Fonseca, N. L. Delgado-Buenrostro, E. B. Gutiérrez-Cirlos, C. M. Calderón-Torres, T. Cabellos-Avelar, Y. Sánchez-Pérez, E. Pinzón, I. Torres, E. Molina-Jijón, C. Zazueta, *Toxicol. Lett.* **2011**, *202*, 111.
[28] C. Egbuna, V. K. Parmar, J. Jeevanandam, S. M. Ezzat, K. C. Patrick-Iwuanyanwu, C. O. Adetunji, J. Khan, E. N. Onyeike, C. Z. Uche, M. Akram, *J. Toxicol.* **2021**, *2021*, 9954443.
[29] S. Patiño, J. Grace, *Plant, Cell Environ.* **2002**, *25*, 41.
[30] B. H. Matthews, A. N. Alsante, S. D. Brooks, *ACS Earth Space Chem.* **2023**, *7*, 1207.
[31] P. Duan, W. Hu, Z. Wu, K. Bi, J. Zhu, P. Fu, *Atmos. Res.* **2023**, *285*, 106659.
[32] T.-F. Fan, S. Park, Q. Shi, X. Zhang, Q. Liu, Y. Song, H. Chin, M. S. B. Ibrahim, N. Mokrzecka, Y. Yang, *Nat. Commun.* **2020**, *11*, 1449.
[33] T. Hornick, A. Richter, W. S. Harpole, M. Bastl, S. Bohlmann, A. Bonn, J. Bumberger, P. Dietrich, B. Gemeinholzer, R. Grote, *Plants, People, Planet* **2022**, *4*, 110.
[34] T.-F. Fan, M. G. Potroz, E.-L. Tan, M. S. Ibrahim, E. Miyako, N.-J. Cho, *Sci. Rep.* **2019**, *9*, 9626.
[35] Z. Zhao, Y. Hwang, Y. Yang, T. Fan, J. Song, S. Suresh, N.-J. Cho, *Proc. Natl. Acad. Sci.* **2020**, *117*, 8711.
[36] Z. Zhao, J. Kumar, Y. Hwang, J. Deng, M. S. B. Ibrahim, C. Huang, S. Suresh, N.-J. Cho, *Proc. Natl. Acad. Sci.* **2021**, *118*, 2113715118.
[37] Z. Zhao, J. Deng, H. Tae, M. S. Ibrahim, S. Suresh, N. J. Cho, *Adv. Mater.* **2022**, *34*, 2109367.
[38] M. Wurdack, N. Lundt, M. Klaas, V. Baumann, A. V. Kavokin, S. Höfling, C. Schneider, *Nat. Commun.* **2017**, *8*, 259.
[39] Q. Shi, M. S. B. Ibrahim, X. Zhang, Y. Hwang, H. Chin, S. Chen, W. S. Tan, H. Li, J. Song, N.-J. Cho, *Appl. Mater. Today* **2022**, *27*, 101471.
[40] K.-T. Lin, J. Han, K. Li, C. Guo, H. Lin, B. Jia, *Nano Energy* **2021**, *80*, 105517.
[41] H. Zhang, T. Wei, Q. Zhang, W. Ma, P. Fan, D. Salamon, S.-T. Zhang, B. Nan, H. Tan, Z.-G. Ye, *J. Mater. Chem. C* **2020**, *8*, 16648.
[42] F.-X. Xiao, M. Pagliaro, Y.-J. Xu, B. Liu, *Chem. Soc. Rev.* **2016**, *45*, 3088.
[43] M. J. Kelly, D. E. Wolfe, J. Singh, J. Eldridge, D. M. Zhu, R. Miller, *Int. J. Appl. Ceram. Technol.* **2006**, *3*, 81.
[44] J. Mandal, Y. Fu, A. C. Overvig, M. Jia, K. Sun, N. N. Shi, H. Zhou, X. Xiao, N. Yu, Y. Yang, *Science* **2018**, *362*, 315.
[45] Y. Deng, Y. Yang, Y. Xiao, H. L. Xie, R. Lan, L. Zhang, H. Yang, *Adv. Funct. Mater.* **2023**, *33*, 2301319.
[46] K. Lin, S. Chen, Y. Zeng, T. C. Ho, Y. Zhu, X. Wang, F. Liu, B. Huang, C. Y.-H. Chao, Z. Wang, *Science* **2023**, *382*, 691.
[47] KMA National Climate Data Center, data.kma.go.kr (accessed: December 2022).
[48] National Environment Agency, https://www.nea.gov.sg/corporate-functions/weather (accessed: July 2023).
[49] J. Fei, D. Han, J. Ge, X. Wang, S. W. Koh, S. Gao, Z. Sun, M. P. Wan, B. F. Ng, L. Cai, *Adv. Funct. Mater.* **2022**, *32*, 2203582.

 © 2025 Wiley-VCH GmbH

16163028, 0, Downloaded from https://advanced.onlinelibrary.wiley.com/doi/10.1002/adfm.202511893 by NANYANG TECHNOLOGICAL UNIVERSITY, Wiley Online Library on [21/07/2025]. See the Terms and Conditions (https://onlinelibrary.wiley.com/terms-and-conditions) on Wiley Online Library for rules of use; OA articles are governed by the applicable Creative Commons License